2003

Inversion for sediment geoacoustic properties at the New England Bight

Gopu R. Potty
University of Rhode Island, gpotty@uri.edu

James H. Miller
University of Rhode Island, miller@uri.edu

See next page for additional authors

Citation/Publisher Attribution
Potty, G. R., Miller, J. H., & Lynch, J. F. (2003). Inversion for sediment geoacoustic properties at the New England Bight. *The Journal of the Acoustical Society of America, 114*(4), 1874-1887. doi: 10.1121/1.1605391
Available at: https://doi.org/10.1121/1.1605391

Inversion for sediment geoacoustic properties at the New England Bight

Gopu R. Potty, James H. Miller, and James F. Lynch

Citation: The Journal of the Acoustical Society of America **114**, 1874 (2003); doi: 10.1121/1.1605391
View online: https://doi.org/10.1121/1.1605391
View Table of Contents: http://asa.scitation.org/toc/jas/114/4
Published by the Acoustical Society of America

Inversion for sediment geoacoustic properties at the New England Bight

Gopu R. Potty[a] and James H. Miller
Department of Ocean Engineering, University of Rhode Island, Narragansett, Rhode Island 02882

James F. Lynch
Woods Hole Oceanographic Institution, Woods Hole, Massachusetts 02543

(Received 15 May 2002; revised 25 June 2003; accepted 14 July 2003)

This article discusses inversions for bottom geoacoustic properties using broadband acoustic signals obtained from explosive sources. Two different inversion schemes for estimating the compressional wave speeds and attenuation are presented in this paper. In addition to these sediment parameters, source–receiver range is also estimated using the arrival time data. The experimental data used for the inversions are SUS charge explosions acquired on a vertical hydrophone array during the Shelf Break Primer Experiment conducted south of New England in the Middle Atlantic Bight in August 1996. The modal arrival times are extracted using a wavelet analysis. In the first inversion scheme, arrival times corresponding to various modes and frequencies from 10 to 200 Hz are used for the inversion of compressional wave speeds. A hybrid inversion scheme based on a genetic algorithm (GA) is used for the inversion. In an earlier study, Potty *et al.* [J. Acoust. Soc. Am. **108**(3), 973–986 (2000)] have used this hybrid scheme in a range-independent environment. In the present study results of range-dependent inversions are presented. The sound speeds in the water column and bathymetry are assumed range dependent, whereas the sediment compressional wave speeds are assumed range independent. The variations in the sound speeds in the water column are represented using empirical orthogonal functions (EOFs). The replica fields corresponding to the unknown parameters were constructed using adiabatic theory. In the second inversion scheme, modal attenuation coefficients are calculated using modal amplitude ratios. The ratios of the modal amplitudes are also calculated using time-frequency diagrams. A GA-based inversion scheme is used for this search. Finally, as a cross check, the computed compressional wave speeds along with the modal arrival times were used to estimate the source–receiver range. The inverted sediment properties and ranges are seen to compare well with *in situ* measurements and historical data.
 [DOI: 10.1121/1.1605391]

PACS numbers: 43.30.Pc, 43.30.Ma, 43.30.Bp [WLS]

I. INTRODUCTION

Acoustic propagation in shallow water is greatly influenced by the properties of the bottom. Indirect methods for the estimation of bottom properties have been given much attention in underwater acoustics as direct measurements (e.g., cores) are very hard to make. In this article we discuss two different inversion schemes for the estimation of sediment compressional wave speeds and compressional attenuation using broadband data. In inversion scheme I, sediment compressional wave speeds are estimated using a hybrid inversion scheme based on the dispersion behavior of broadband acoustic propagation. The application of this inversion scheme to a range-independent environment is discussed in detail by Potty *et al.* (2000) in a previous article. This hybrid scheme is a combination of a genetic algorithm (GA) and the Levenberg–Marquardt optimization method. Compressional wave attenuation values are estimated using inversion scheme II based on modal amplitude ratios. In addition to the sediment properties, other parameters such as bathymetry, source depth, receiver depth, range, and source level are also treated as unknowns in this inversion scheme. The relative importance of these parameters is assessed by a sensitivity study. This latter inversion scheme is also carried out using a GA.

When a broadband acoustic source is used in shallow-water waveguide, the acoustic propagation exhibits dispersion effects. The group velocities, i.e., the speeds at which energy is transported, differ for different frequencies and modes. This dispersion effect can be observed by time–frequency analysis of an acoustic signal recorded at sufficiently large distance away from the source. The times of arrivals of different modes at various frequencies can be directly extracted from these time–frequency distributions. Lynch, Rajan, and Frisk (1991) successfully used dispersion characteristics for the inversion of geoacoustic properties using linear perturbation methods. Nonlinear inverse methods for estimating bottom properties were subsequently developed by Collins *et al.* (1992), Gerstoft *et al.* (1996), and others. It should be noted that dispersion analysis of seismic interface waves has been used extensively to determine the shear properties of near-bottom ocean sediments (Jensen and Schmidt, 1985; Caiti *et al.*, 1994; Stoll *et al.*, 1994). Turning to the New England Shelf Break environment, Potty *et al.* (2000) have recently used global optimization methods for

[a]Electronic mail: potty@oce.uri.edu

 0001-4966/2003/114(4)/1874/14/$19.00

their geoacoustic inversion in the range-independent shallow-water environment case. Their genetic algorithm-based inversion gave good estimates for sediment compressional wave speeds, which matched well with deep core data [Atlantic Margin Coring (AMCOR) Project] and shallow gravity cores at the same location. In this article we extend this inversion scheme to the mildly range-dependent environment using adiabatic theory.

The recovery of range-dependent structures in the ocean environment has been a subject of interest in ocean acoustics. Tolstoy *et al.* (1991) proposed a linearized matched field processing approach to acoustic tomography, assuming adiabatic normal-mode propagation for low-frequency signals received on vertical arrays. Taroudakis and Marakaki (1997) used GAs and modal phases to invert for a range-dependent environment due to a cold eddy using adiabatic theory. Siderius, Gerstoft, and Nielsen (1998) have used GAs for geoacoustic inversion in a range-dependent environment.

Turning to the estimation of medium attenuation, Tindle (1982) and Zhou *et al.* (1987) used modal amplitude ratios to extract modal attenuation coefficients. Using this approach they were able to model the nonlinear frequency dependence of the acoustic attenuation in the upper sediment layer in a shallow-water location in the Yellow Sea. Rajan, Frisk, and Lynch (1992) estimated modal attenuation coefficients using various methods based on the pressure field or its Hankel transform. The bottom attenuation profile is obtained from these modal attenuation coefficients by solving an integral equation using linear inverse theory. They also separated contributions from other attenuating mechanisms (shear, rough surface scattering, etc.). In this article, an inverse scheme for attenuation is presented which utilizes the compressional wave-speed values determined using the dispersion-based inversion. This scheme calculates the modal attenuation coefficients based on modal amplitude ratios and transmission loss data. In addition to modal attenuation coefficients, source depth, receiver depth, range, and source levels are treated as unknowns in the inversion and checked for consistency.

Our study is arranged as follows. Sediment compressional wave speeds are first addressed in this study, using inversion scheme I based on the group speed dispersion. Section II A contains the details of this inversion scheme. Section II B begins by presenting inversion scheme II for compressional wave attenuation. This inversion scheme is applied to synthetic data as well as field data from the Shelf Break Primer Experiment. Next, the group speeds estimated using the inversion scheme and the arrival times obtained from the field data are used to estimate the source–receiver ranges assuming range independence. Section II C briefly explains this source distance estimation method.

A mode-based sensitivity study, performed to assess the relative influence of various parameters (compressional wave speed, ocean sound speed, and water depth), is discussed in Sec. III A. Sensitivity of group speeds to these parameters is discussed in Sec. III B and sensitivity of modal amplitude ratios in Sec. III C. Section IV A presents the details of the Shelf Break Primer Experiment. Section IV B contains the description of the historic geoacoustic data pertaining to the experimental region. Section V contains the major new results of this study. Section V A shows the results of compressional speed inversion, Sec. V B discusses the results of range estimation, and Sec. V C contains result of attenuation estimates. Section VI summarizes and concludes the article.

II. INVERSION SCHEMES

We use a genetic algorithm (Goldberg, 1988) as the basic search tool for our inversion of sediment compressional wave speeds and attenuation. The principle of the GA is simple and closely resembles the genetic cycle. From all the possible parameter vectors, an initial population of members is randomly selected. The ''fitness'' of each member is computed on the basis of an objective function. Based on the fitness of the members, a set of ''parents'' is selected and through a randomization procedure a set of ''children'' is produced. These children replace the least fit of the original population and the process iterates to develop an overall fitter population. A hybrid scheme is used in the inversion for sediment compressional wave speeds, where the best parameter vector obtained using the GA is further optimized using a local search. The Levenberg–Marquardt algorithm (Fletcher, 1980) was employed for this local search. By applying this method at the end of the GA search, we can both assess the quality of the GA solution locally and also search for a better solution. Error bounds on the parameters were also estimated using two different approaches. During the optimization using GA, all the population is stored and is later used to estimate *a posteriori* probabilities. In addition to the best possible estimate, moments of the *a posteriori* distributions such as mean and covariance can also be estimated. This error estimation procedure is discussed in detail by Gerstoft (1994) and Potty *et al.* (2000). These error estimates provide a measure of the convergence of the optimization procedure and can be used to make comparisons between retrieved parameters. Added to this *a posteriori* error estimate, the quality of the inversion is also examined locally by numerically calculating the standard deviation using the Hessian matrix (Sen and Stoffa, 1995). Elements of the Hessian matrix are the second partial derivatives of the objective function with respect to the model parameters. They are local estimates that only characterize the region about the model at which they are calculated and are numerically evaluated in the neighborhood of the best solution. Hessian uncertainty will represent the true uncertainty if the best solution corresponds to the true model. The ability of the global approaches to efficiently navigate the multipeaked and noisy search space and to converge to the true solution increases the effectiveness of the Hessian approach. It should be noted that this Hessian method assumes that the error surface is Gaussian.

A. Method of inversion for sediment compressional speeds: Inversion scheme I

In this section, we discuss our inversion for sediment compressional wave speed. The sound speed in the water column and bathymetry are considered range dependent, whereas the sediment compressional wave speed is treated as range independent in this inversion. This is because we have

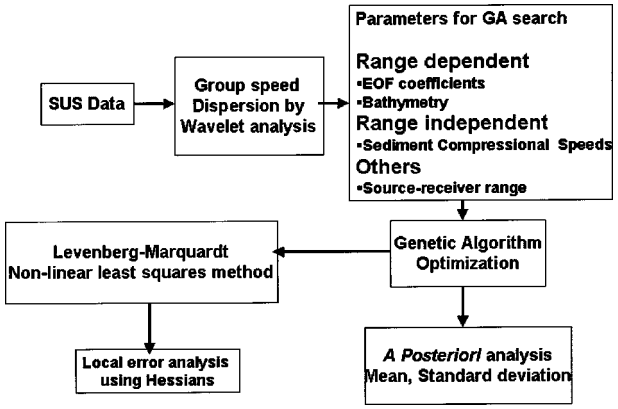

FIG. 1. Steps involved in the inversion scheme I. The source–receiver range is divided into five sections in which the bathymetry and water column sound speeds are allowed to vary.

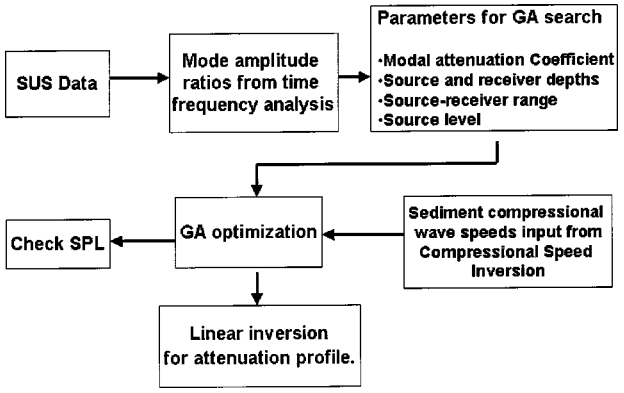

FIG. 2. Steps involved in the inversion scheme II. Sound speeds in the water column and the compressional speeds in the sediment are obtained from a previous inversion by Potty *et al.* (2000).

a priori information about the range dependence of the water column sound speed and bathymetry. Shear effects in the sediment are neglected, as shear speeds are expected to be of the order of 150 m/s (Hamilton, 1980) for the type of sediments present at the experimental location. In the inversion scheme to estimate the sediment compressional wave speeds, the parameter vectors searched for consisted of coefficients of empirical orthogonal functions (EOFs) of water column sound speed, the bathymetry, and the source to receiver range, in addition to the sediment compressional wave-speed profile.

The objective function for the inversion was based on the minimization of group speed differences, and was of the form

$$E(m)=\sum_i \frac{[d_i-F_i(m)]^2}{\sigma_i^2}. \tag{1}$$

In Eq. (1), $E(m)$ is the objective function for the parameter vector m and σ_i is the standard deviation associated with the ith data point. The numerator of this equation represents the mismatch between the observed data $(d,N\times 1)$ and the prediction $[F(m),N\times 1]$ of the forward model. A normal-mode routine is used to calculate the predictions $[F(m)]$. The major steps involved in this inversion scheme are shown in Fig. 1.

B. Method of inversion for the compressional wave attenuation coefficient: Inversion scheme II

The compressional wave attenuation is estimated in this paper assuming range-independent propagation. In a range-independent environment, the acoustic pressure at range r in the far field can be expressed as a sum of M normal modes

$$P(r,z)=\frac{e^{i\pi/4}}{\rho(z_s)\sqrt{8\pi r}}\sum_{m=1}^{M}\frac{\psi_m(z_s)\psi_m(z)(e^{(i\kappa_{rm}-\beta_m)r})}{\sqrt{\kappa_{rm}}}, \tag{2}$$

where $P(r,z)$ is the acoustic pressure at a range r and at depth z, z_s is the depth of the source, ψ_m is the mth mode function, κ_{rm} is the horizontal wave number, and β_m is the modal attenuation coefficient. At a given range r from the source, the ratio of the amplitude of the second mode to the amplitude of the first mode can be written as

$$R_{21}(f)=\sqrt{\frac{\kappa_1}{\kappa_2}}\left|\frac{\psi_2(z_s)\psi_2(z)}{\psi_1(z_s)\psi_1(z)}\right|e^{(\beta_1-\beta_2)r}. \tag{3}$$

Ratios of spectral amplitudes between other modes also can be similarly expressed.

Modal attenuation coefficients were inverted by minimizing the difference between the theoretical spectral ratios computed using Eq. (3) and the experimental spectral ratios calculated from time–frequency diagrams in a least-squares sense. The modal amplitude ratios corresponding to the first three modes $[R_{21}(f),\ R_{31}(f),$ and $R_{23}(f)]$ are obtained by time–frequency analysis using wavelet-based methods. The mode functions (ψ) and eigenvalues (κ) are obtained using a standard normal-mode routine. The sound-speed profile obtained from the inversion done previously (Potty *et al.*, 2000) is used for this purpose. The unknowns in the inversion scheme are the source depth (z_s), receiver depth (z), the range (r), and the modal attenuation coefficients $(\beta_1,\ \beta_2,$ and $\beta_3)$. As a check, transmission loss is calculated using the inverted modal attenuation coefficients and compared with experimental values. The source level of the explosion is also treated as unknown. A genetic algorithm (GA) was used to perform this inversion.

Having obtained the modal attenuation coefficients using this inversion, the compressional wave attenuation profile is determined from the integral equation

$$\kappa_{rm}\beta_m=\int_0^\infty \alpha(z)k(z)|\psi_m(z)|^2dz, \tag{4}$$

where $k(z)$ is the wave number and $\alpha(z)$ is the attenuation profile. We solve this equation using linear inverse theory (Rajan *et al.*, 1987). The ability of this method to estimate the attenuation profile depends primarily on the amplitudes of the mode functions at various depths. The mode function falls off exponentially with depth beyond the turning depth, and hence this method will not be able to estimate the attenuation coefficient reliably at depths much greater than the turning depth. The steps involved in the inversion scheme are shown in Fig. 2. This inversion scheme is first tested using synthetic data generated for a known sound-speed profile and attenuation.

C. Method of estimating the source–receiver ranges from mode arrival times

The source–receiver range (r) can be evaluated from the arrival time difference between two frequencies at a single mode or from two modes at a single frequency. This serves as a cross check for the compressional wave-speed inversions. The arrival time difference between two frequencies for any given mode i at range r is given by

$$\Delta T_{ii}(f)=\left[\frac{1}{V_g^i(f)}-\frac{1}{V_g^i(f_H)}\right]r, \tag{5}$$

where f_H is a reference frequency which is different from f. At a distance r, for the same frequency the arrival time difference between mode j and mode i is given by

$$\Delta T_{ji}(f)=\left[\frac{1}{V_g^j(f)}-\frac{1}{V_g^i(f)}\right]r, \quad i\neq j. \tag{6}$$

These equations are of the form

$$\Delta T(f)=[K_t(f)]r, \tag{7}$$

in which ΔT is the experimental travel time differences [left-hand side of Eqs. (5) and (6)] and K_t is the theoretical group slowness differences [the quantity within brackets in the right-hand sides of Eqs. (5) and (6)]. The group speeds (V_g) calculated theoretically using the compressional speed inversion and arrival time differences ΔT obtained from the experimental data are used to calculate the range r. It should be noted that these equations are applicable only to range-independent environments, so that errors will be incurred if the environment contains range dependence.

III. SENSITIVITY STUDY

A. Mode-based sensitivity study

In order to prepare for our inversion, the relative importance of sound speed in water column (cw), compressional speeds in four layers of sediments [cp1 (0–6 m), cp2 (6–12 m), cp3 (12–18 m), and cp4 (18–24 m)] each 6 m thick, and the water depth was analyzed using a mode-based sensitivity study. These values were then compared with sensitivities calculated based on group speed changes due to changes in the above parameters. The mode-based sensitivity study is described in detail by Kessel (1999) and is applicable to weakly range-dependent environments. Some of the important aspects of this study are included in this section.

A possible measure of sensitivity can be written in terms of the change in the pressure field due to some environmental changes relative to a suitable norm as $\Delta P(x,x_s)/\|P(x,x_s)\|$. Here, $P(x,x_s)$ is the original pressure and $\Delta P(x,x_s)$ is the change in pressure. If $P'(x,x_s)$ is the new field corresponding to a small change in the environment, the change in pressure can be written as contributions from modes $m=1,2,3,...,M$.

$$\Delta P(x,x_s)=\sum_{m=1}^{M}\left(P'_m(x,x_s)-P_m(x,x_s)\right). \tag{8}$$

Here, $x_s=(r_s,z_s)$ and $x=(r,z)$ define the positions of the source and receiver where r and r_s are horizontal positions of receiver and source, respectively. z and z_s represent the receiver and source depths, respectively. The overall tendency of the perturbation $|\Delta P(x,x_s)|^2$ can be represented by the incoherent mode sum

$$|\Delta P(x,x_s)|^2_{\text{incoh}}=\sum_{m=1}^{M}|P'_m|^2+|P_m|^2-2\,\text{Re}(P'_mP^*_m), \tag{9}$$

in which * denotes complex conjugation. Noting that the long-range horizontal phase $e^{i\xi_mR}$ of the modes is the most sensitive part of the field to changes in environment, we can write

$$P'_m(x,x_s)\approx P_m(x,x_s)e^{i\Delta\xi_mR}, \tag{10}$$

where

$$\Delta\xi_m=\xi'_m-\xi_m. \tag{11}$$

In order to evaluate the sensitivity for a given environmental change, the local wave numbers κ_m and κ'_m corresponding to original and modified environments, respectively, for each mode m are calculated. Corresponding changes in the modal phase ($\Delta\xi_m$) are computed using these wave numbers

$$\xi_m=\frac{1}{r-r_s}\int_{r_s}^{r}\kappa_m(r)dr, \tag{12}$$

and

$$\xi'_m=\frac{1}{r-r_s}\int_{r_s}^{r}\kappa'_m(r)dr. \tag{13}$$

It should also be noted that, if the medium absorbs energy, then ξ_m is complex

$$\xi_m=\gamma_m+i\alpha_m. \tag{14}$$

The perturbation in the field can now be written as

$$|\Delta P(x,x_s)|^2_{\text{incoh}}=\sum_{m=1}^{M}|P'_m|^2\Omega_m(r,r_s), \tag{15}$$

in which

$$\Omega_m(r,r_s)=1+e^{-2\Delta\alpha_mR}-2e^{-\Delta\alpha_mR}\cos\Delta\gamma_mR. \tag{16}$$

It should also be noted that, in order to isolate the role of long-range horizontal phase, $\Delta\alpha_m$ may be taken as zero. The mean of this perturbation over a large number of source–receiver positions will then be

$$\overline{|\Delta P(x,x_s)|^2_{\text{incoh}}}=\|p(r,r_s)\|^2\overline{\Omega(r,r_s)}, \tag{17}$$

in which $\overline{\Omega(r,r_s)}$ is a weighted average over modes as shown below (Kessel, 1999)

$$\overline{\Omega(r,r_s)}=\frac{1}{\|p(r,r_s)\|^2}\sum_{m=1}^{M}\overline{|p_m|^2}\Omega_m(r,r_s). \tag{18}$$

If we use N source–receiver positions $x_s^n=(r_s,z_s^n)$ and $x^n=(r,z^n)$ $(n=1,2,3,...,N)$, respectively, then

$$\overline{|P_m|^2}=\frac{1}{N}\sum_{n=1}^{N}|P_m(x^n,x_s^n)|^2, \tag{19}$$

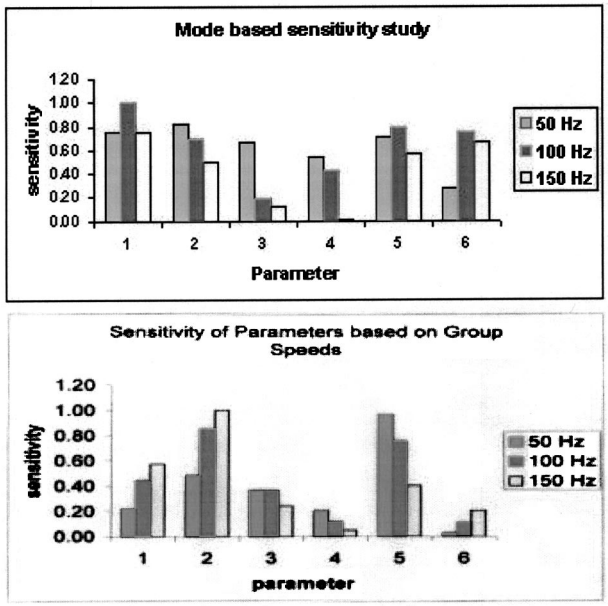

FIG. 3. Sensitivity of sediment compressional speeds at 0–6 m (parameter 1), 6–12 m (parameter 2), 12–18 m (parameter 3), 18–24 m (parameter 4). Parameter 5 corresponds to changes in water depth and parameter 6 indicates ocean sound-speed variations. Top panel shows the sensitivities calculated based on the mode-based sensitivity study. Sensitivities shown in the bottom panel were calculated based on the changes in group speeds.

and

$$\|p(r,r_s)\|^2=\overline{|p_m|^2} \tag{20}$$

(r_s,z_s) and (r,z) are the horizontal and vertical positions of the source and receiver such that the range $R=|r-r_s|$.

The top panel in Fig. 3 shows the sensitivities of these parameters for frequencies of 50, 100, and 150 Hz. The sound-speed profile obtained by the compressional wave-speed inversion scheme (Potty *et al.*, 2000) was used for this analysis. The sediment compressional speeds at depths 0–6 m (cp1), 6–12 m (cp2), 12–18 m (cp3), and 18–24 m (cp4) were changed by ±30 m/s, water depth by ±4 m, and ocean sound speed (cw) by ±3 m/s. These sensitivity values are scaled relatively, larger values indicating higher sensitivity for the changes in the parameters as mentioned above. For the given changes in compressional speeds, ocean sound speed, and water depth the sensitivities are nearly equal. Water depth variations have equal sensitivities for the three frequencies considered, which are comparable to the sensitivities of all the other parameters in magnitude. The sensitivities also show the expected dependence on frequency. At the lower frequency (50 Hz) changes in compressional speeds at deeper sediment depths are very sensitive, whereas at 150 Hz the sensitivity is very low at deeper sediment depths. At higher frequencies, the ocean sound speed and water depth are more sensitive than deep sediment compressional speeds. At 50 Hz, sound speed in the water column has comparatively less effect than the other parameters.

B. Sensitivity of group speeds

The bottom panel in Fig. 3 shows the sensitivities calculated based on the changes in group speeds corresponding to changes in parameters mentioned earlier. The magnitudes of these changes were same as in the mode-based sensitivity study. The group speeds seem to be more sensitive to changes in water depth and compressional wave speeds at depths 0–6, and 6–12, and 12–18 m. Unlike the mode-based sensitivity study, frequencies 100 and 150 Hz are more effective at depths 0–6 and 6–12 m. This may be due to the fact that more modes are included at higher frequencies compared to 50 Hz. These results are identical to the results of the sensitivity study reported by Potty *et al.* (2000).

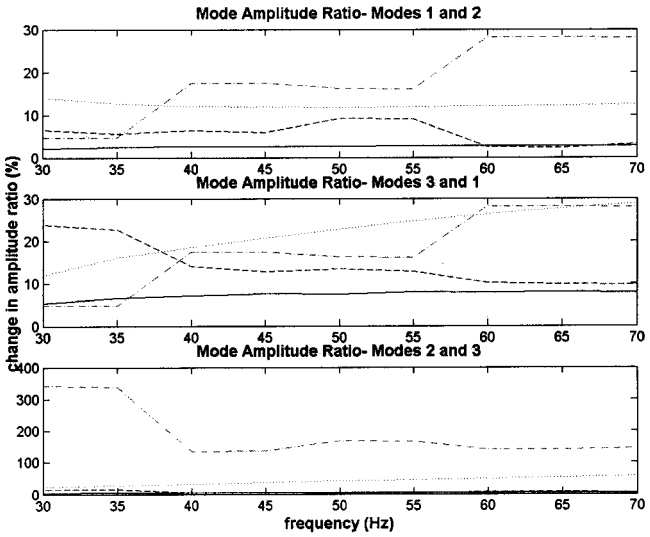

FIG. 4. Effect of variations in the source depth, receiver depth, range, and modal amplitude ratio on the spectral ratios. Solid line indicates variations due to 1.5-m source depth increase from baseline, dotted line indicates 1.5-m increase in receiver depth, dash dot line 30% increase in beta, and dashed line indicates 1.5-km increase in range. The top, middle, and bottom panels show the ratio of modes 1 and 2, modes 1 and 3, and modes 2 and 3, respectively.

C. Sensitivity of modal amplitude ratios

A sensitivity study was performed to understand the effect of model parameters on the spectral amplitude ratios. Figures 4 and 5 show the influences of source depth, receiver depth, modal attenuation coefficient, and range on modal amplitude ratios. This analysis was done using the sound-speed profile obtained from the inversion for sediment compressional speeds (Potty *et al.*, 2000). Figure 4 shows the variation of modal amplitude ratios with changes in source depth (+1.5 m), receiver depth (+1.5 m), range (+1.5 km), and modal attenuation coefficient (+30%) from the baseline model. The baseline model corresponds to a source depth of 18 m, receiver depth of 66 m, and at a range of 41 km. Figure 5 shows the variations in modal amplitude ratios with changes in source depth (−1.5 m), receiver depth (−1.5 m), range (−1.5 km), and modal attenuation coefficient (−30%) from the baseline model. The changes in the modal amplitude ratio of mode 3 to mode 1 seem to be comparatively higher than the ratios of modes 2 to 1 and modes 2 to 3. The effect of receiver depth variation is more prominent when compared to source depth variation (Figs. 4 and 5). A ±30% change in modal attenuation coefficient produces far higher variations in modal amplitude ratios, when compared to reasonable changes in range and source depth. Considering the

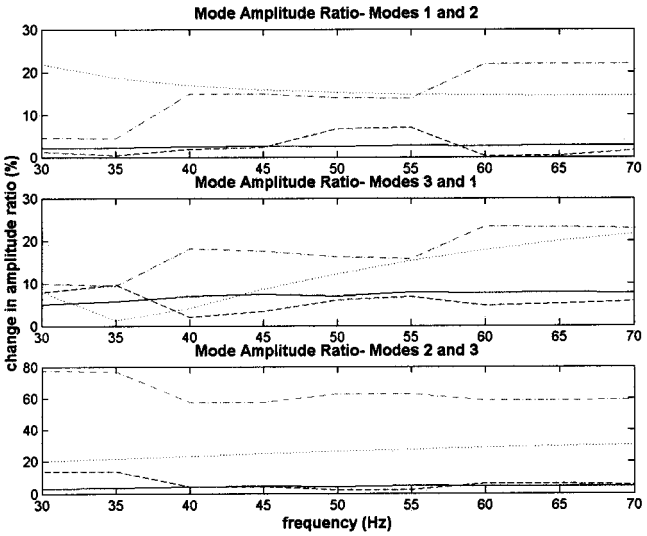

FIG. 5. Effect of variations in the source depth, receiver depth, range, and modal amplitude ratio on the spectral ratios. Solid line indicates variations due to 1.5-m source depth decrease from baseline, dotted line indicates 1.5-m decrease in receiver depth, dash dot line 30% decrease in beta, and dashed line indicates 1.5-km decrease in range. The top, middle, and bottom panels show the ratio of modes 1 and 2, modes 1 and 3, and modes 2 and 3, respectively.

influence of source depth, depth of receiver, and range, all three of these parameters were included as unknowns in the inversion scheme for determining the modal attenuation coefficients.

IV. PRIMER FIELD STUDY

A. General description of the Shelf Break PRIMER experiment

In the summer of 1996, a number of oceanographic and acoustic measurements were taken on the shelf break south of New England in the Middle Atlantic Bight (Fig. 6). Details of the experiment, with emphasis on bottom inversion, are discussed by Potty *et al.* (2000). The SUS component of the experiment involved acquisition of broadband acoustic data on two vertical line arrays (VLAs) on the northeast (NE) and northwest (NW) corners of the experimental area. The SUS charges were of type MK61 and consisted of 0.82 kg of TNT set to detonate at a depth of 18 m. About 80 charges were dropped on the continental shelf and slope in water depths varying from 85 to 300 m. In this study acoustic signals from SUS explosions in the shelf area received at the NE VLA are used to invert for geoacoustic parameters. The positions of these SUS drops and the location of the NE VLA are shown in Fig. 7. The three SUS explosions D2, D4, and D6 are part of the down-slope run, whereas C6 and C9 are part of the cross-slope run. Signals received from these shots on the NE vertical array were analyzed in the present study for compressional wave speed. The NE VLA consisted of 16 hydrophones spanning the water column from a depth of 45.42 to 92.72 m. Data were acquired on the receivers at a sampling frequency of 1395.1 samples/second. Signals from D1 and D2 are used to calculate the modal attenuation coefficients.

The acoustic signal received at the VLA is analyzed using wavelet-based methods to produce time–frequency dispersion diagrams. The advantage of analyzing the signal with wavelets as analyzing kernels is that it enables us to study features of the signal locally with a detail matched to their scale, i.e., broad features on a large scale and fine features on a small scale. This enables us to get the time of arrivals corresponding to higher modes with good resolution. This becomes important since the higher modes penetrate farther into the sediment and hence enable us to invert for deeper sediment properties. The arrival times corresponding to spectral peaks for the various modes at different frequencies are picked from the time–frequency scalograms. It should be noted that there might be multiple peaks corresponding to bubble pulses generated by the explosion. This sometimes makes the identification of the peaks and their corresponding arrival times difficult for various modes. This is a serious problem for the early arrivals above 70 Hz where the arrivals corresponding to various modes are closer.

Figure 8 shows the modal dispersion for four SUS signals (D2, D4, C6, and C9) received at 45.42 m at the NE VLA. The SUS signals C6 and C9 are closer to the VLA compared to the other two, and hence the arrivals are not as well spread out in time. From these wavelet scalograms arrival time data corresponding to individual modes can be extracted, especially those corresponding to late arrivals. The arrival pattern is similar at other depths, except that the relative strengths of the modes differ at these depths. Modes 1 to 9 can be identified from the time–frequency diagram for SUS signal D2. It can also be noted that overall the individual modes are identifiable and well separated, which indicates no major coupling of energy between modes while they propagate. This feature facilitated good quality inversions using this data.

B. Geoacoustic data at the PRIMER site

During the Shelfbreak PRIMER experiment oceanographic parameters such as temperature and salinity were monitored using various methods including SEASOAR (Gawarkiewicz *et al.*, 2001) measurements. These measurements were useful in generating background sound-speed profiles for the ocean and also the empirical orthogonal functions (EOFs) used to represent the sound-speed variations in the ocean. The region adjacent to the PRIMER experimental site has been investigated for sediment properties extensively by many investigators. A detailed review of these studies is presented by Potty *et al.* (2000). The top layer of sediment in the experimental site consists of fine-grained sediments below which sands of fine or medium grain size are found. Only one deeper core (AMCOR Project site 6012) is available within the experimental area. This AMCOR site is down-slope in the southwest corner of the experimental site. Compressional wave-speed profiles have been computed using this core data based on the Biot–Stoll model. Another nearby site is AMCOR 6010, which is on the shelf at a shallower water depth southwest of the experimental site. Trevorrow and Yamamoto (1991) have computed the compressional wave-speed profile at this location. Comparing these two sites, it can be observed that the surface fine-

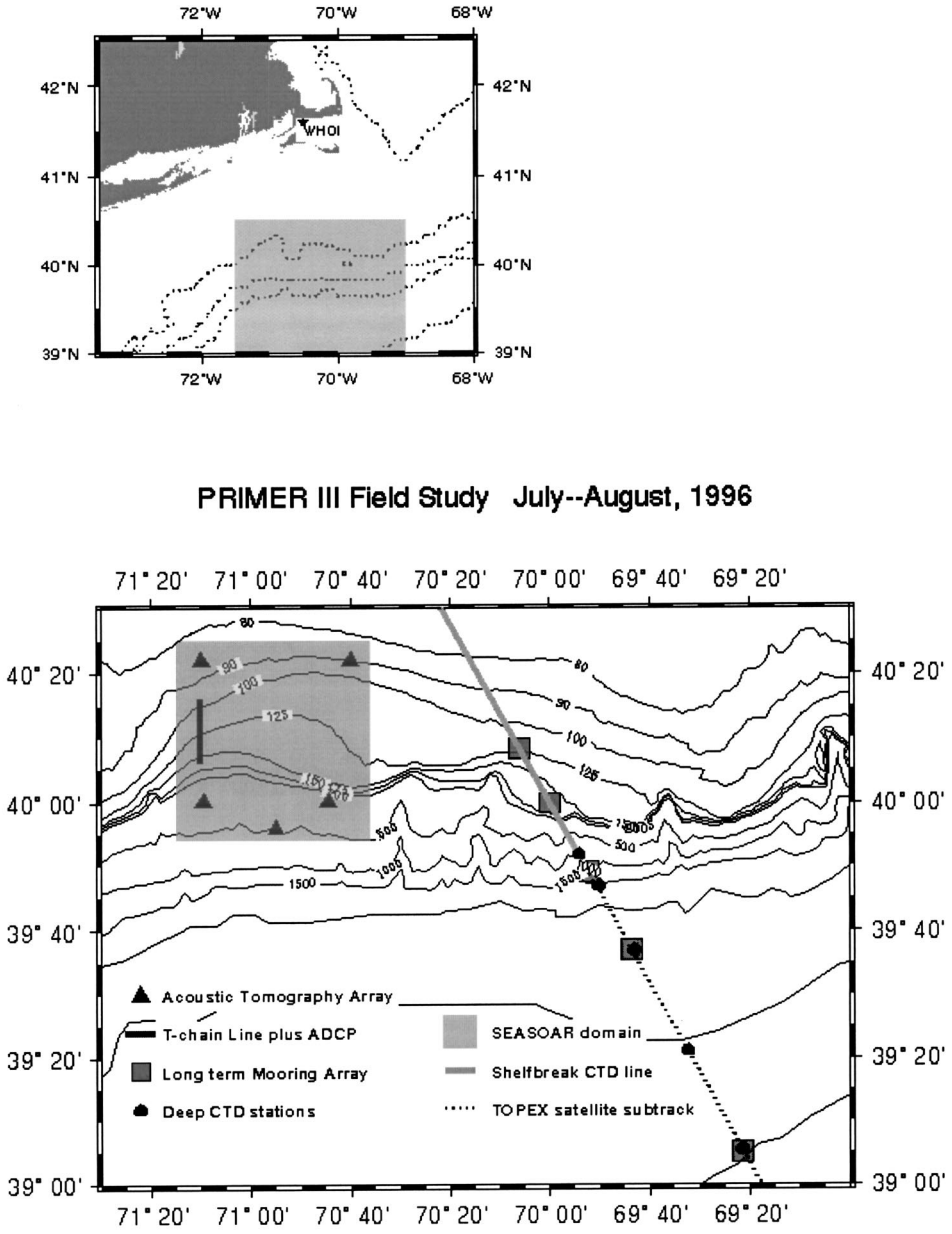

FIG. 6. Location of the PRIMER experimental study.

grained layer becomes thinner along the slope. The mean velocity in the top 10 m of the sediment measured using seismic methods was approximately 1650–1675 m/s (McGinnis and Otis, 1979).

In order to get more data for the top few meters of the sediment, gravity cores were taken in three locations on the shelf at water depths of approximately 90 m, and two more in deeper water depths on the slope (Fig. 7). These cores penetrated down to a maximum depth of 1.5 m in the shelf locations. Beyond this depth the core encountered sandy sediments and refused to penetrate further. For the slope locations the penetration was less due to the presence of the sandy layer at shallower depths. The cores were logged at the Marine Geomechanics Laboratory at the University of Rhode Island to obtain the compressional wave speed, bulk density, and attenuation profiles. It should be noted that these gravity cores give geoacoustic parameters for the top 1–2 m of the sediment only. The present inversion gives compressional speed values down to 25 m depth with reasonable quality. Hence, the gravity cores are useful only to a limited extent for comparison and validation of the present inversion. However, the gravity core data will be much more important for propagation at higher acoustic frequencies.

V. RESULTS AND DISCUSSION

A. Compressional wave-speed inversion: Inversion scheme I

We now pursue the inverse problem. To begin with, the acoustic signals from the SUS charge explosions received at the VLA are now analyzed to evaluate the time–frequency distribution. A signal recorded on a single hydrophone from SUS explosion D2 is shown in Fig. 9. Frequency dispersion is clearly observable even in the raw time series, especially for the later arrivals. We can observe high-frequency late arrivals at 3.5 s after the onset and some low frequencies arriving earlier at around 2.5 s. A Morlet wavelet, commonly used in geophysics and acoustical analysis (Badiey *et al.*,

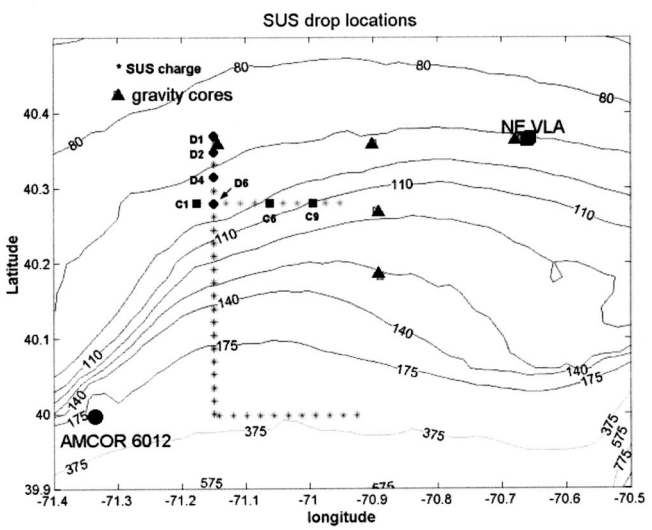

FIG. 7. Location of the SUS charges analyzed in this study. D1, D2, D4, and D6 are part of the down-slope run, whereas C1, C6, and C9 are from the cross-slope run. Locations of the gravity cores and the AMCOR drill site are also shown.

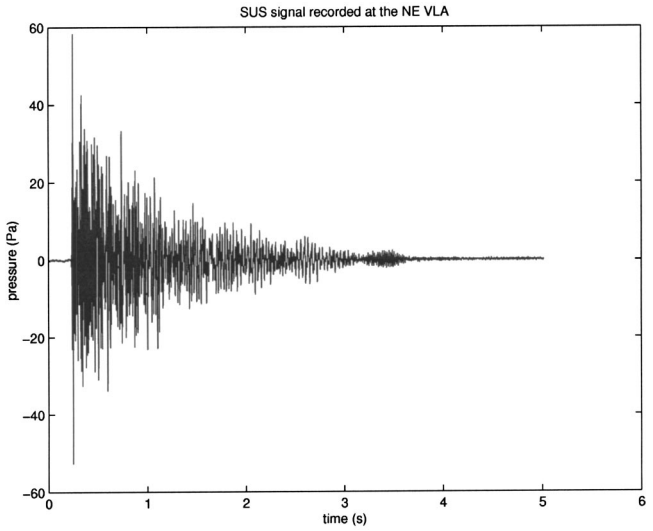

FIG. 9. SUS signal received at the top hydrophone at 45.42-m depth. The source to receiver range is 41 km.

1994), is then used to produce the time–frequency diagram of the signal as shown in Fig. 10. It is seen that the arrivals corresponding to 3.5 and 2.5 s observed in the time series belong to mode 4 and mode 2, respectively. The continuous lines shown in this figure correspond to the theoretical group speed values obtained by the inversion scheme. It should also be noted that, by looking at the time–frequency diagrams for all the receiving hydrophones at various depths along the array, we can extract arrivals for most of the modes. That is, we do not lose modes due to the receiver being in a modal null. The times of arrivals corresponding to the various modes over our range of frequencies were peak picked and used as data for the inversion. The widths of the spectral peaks corresponding to 95% of peak value were also estimated from the time–frequency diagrams. These widths were assumed to represent the uncertainty in the data. Acoustic signals from SUS explosions D2, D4, D6, C6, and C9 were analyzed for time–frequency behavior. All these explosions are in the shelf region and the bathymetry is gently varying. The modes are well defined and there is not much indication of mode coupling.

Forward propagation was modeled using adiabatic theory. In this inversion scheme, the propagation path is divided into five sections. Sediment properties in each section are assumed range independent. Up to nine layers of sediments with different compressional speeds and unequal thickness were considered. Close to the sediment–water interface the layers were very thin compared to deeper depths where penetration of acoustic energy is very low. Empirical orthogonal functions (EOFs) were generated using ocean sound-speed profiles at various locations in the propagation path calculated using SEASOAR temperatures. Four EOF coefficients were used to represent the variations at each section. The water depth at each section and the source–receiver

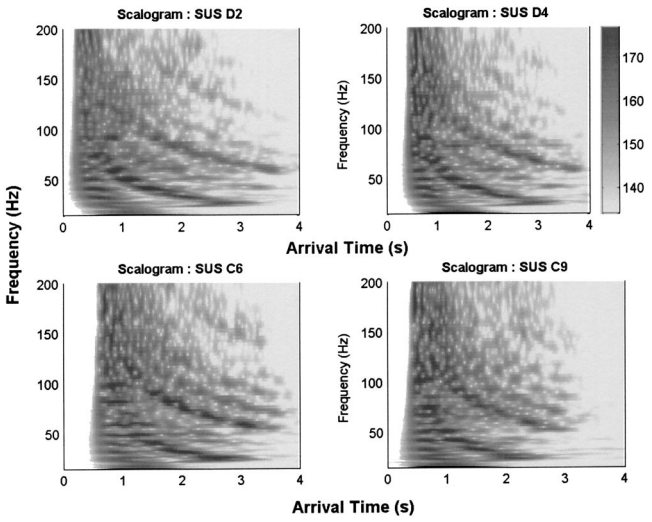

FIG. 8. Dispersion diagrams for four SUS signals received at a depth of 45.42 m. The arrival times are arbitrary. Locations of these SUS drops are shown in Fig. 7.

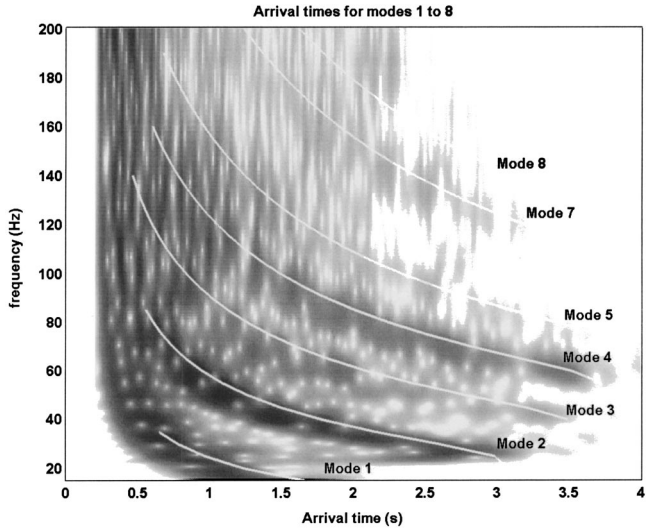

FIG. 10. Comparison of arrival times for SUS signal from D2. The continuous lines are the theoretical group speed curves calculated using the inversion.

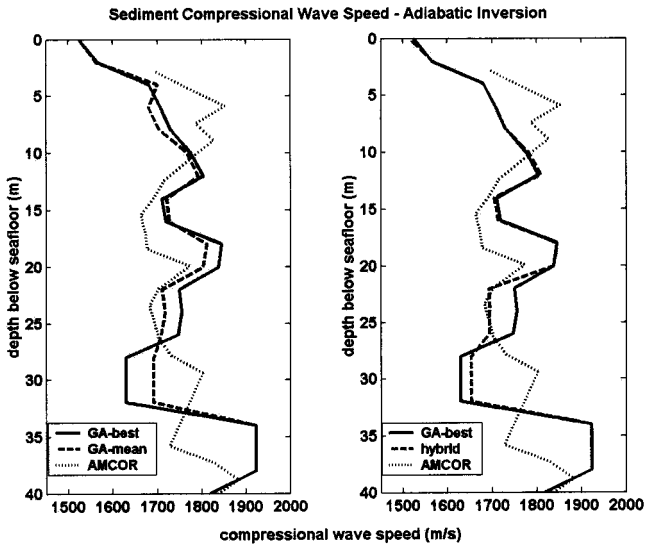

FIG. 11. Sediment compressional speeds obtained by GA inversion (left panel) and hybrid inversion (right panel). Compressional speeds calculated using the AMCOR data are also shown.

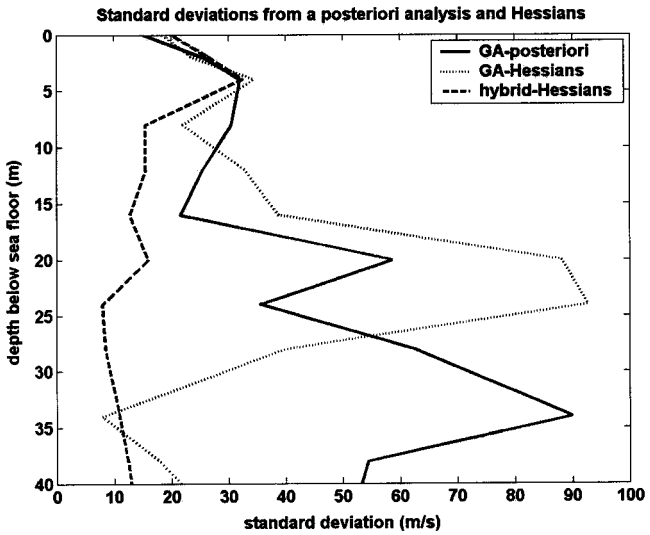

FIG. 12. Standard deviation of the sound-speed estimates computed by *a posteriori* error analysis. Local estimates calculated using Hessians are also shown.

range were also included as unknowns in the inversion scheme for compressional wave speeds. Hence, at each section four EOF coefficients, compressional wave speeds at nine layers, water depth, and range were used to model the environmental and geometric properties. Shear effects in the sediments were neglected. A normal-mode program (Porter and Reiss, 1984) was used to calculate the eigenvalues and mode shapes at each section. The group speed values for various frequencies and modes were calculated and matched with the experimentally observed group speeds. A GA was used to minimize the difference between the modeled and observed group speed values in a least-square sense via the objective function [Eq. (1)]. The GA was used with a stochastic universal sampling selection algorithm, real mutation, and discrete recombination. Three separate runs were made to verify the robustness of the model. The sampled model space is stored and used to calculate the *a posteriori* error estimates. The procedure for the calculation of the error estimates is described in detail by Potty *et al.* (2000).

Figure 11 (left panel) shows the path-averaged compressional wave speeds obtained by the inversion using signals from SUS D2. Compressional wave-speed profiles corresponding to the mean and best parameters obtained by the GA inversion are plotted along with the AMCOR profile for comparison. The inversion agrees with the AMCOR profile reasonably well considering the fact that the AMCOR location is approximately 40 km down slope. The mean and best profiles agree closely for the top 25 m, indicating good convergence at these depths. Figure 11 (right panel) shows the improvements achieved by the application of our hybrid method. It can be noted that the application of Levenberg–Marquardt methods did not produce appreciable improvement in this case, especially in the top 25 m. Figure 12 shows the standard deviations computed using *a posteriori* analysis and Hessians. The standard deviation is of the order of 15–20 m/s in the top 25 m. Down to a depth of 20 m, the Hessians are very high, which indicates very good convergence and explains the lack of success of the hybrid method. It can also be noted that the standard deviation calculated using these two different methods matches very well. Both the methods show very large errors in the 20–25-m depths. The hybrid method was effective at these depths, as it reduces the errors in this region. It should be noted that uncertainty generally increases with depth due to reduced modal penetration at greater depths. Uncertainty calculated by different methods showed this trend at depths greater than 30 m. We also see fluctuations in uncertainty at depths lower than 30 m. This may be due to the fact that different modes penetrate to different depths and hence sample different layers of sediment. This will be more pronounced as we go deep, as the inversion there is based on relatively smaller number of modes.

Figure 13 shows the compressional speed profile in the top 1.4 m of the sediment. Core data obtained from the grav-

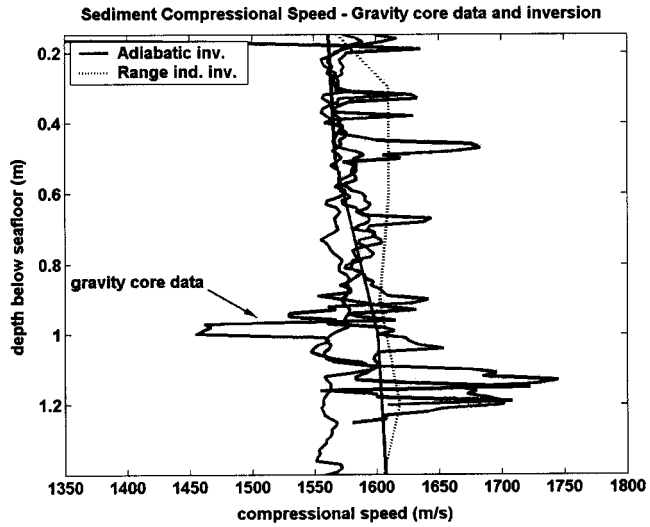

FIG. 13. Sediment compressional speeds obtained by hybrid inversion. Compressional speeds calculated using the gravity core data are also shown. The range-independent inversion shown in the figure is from Potty *et al.* (2000).

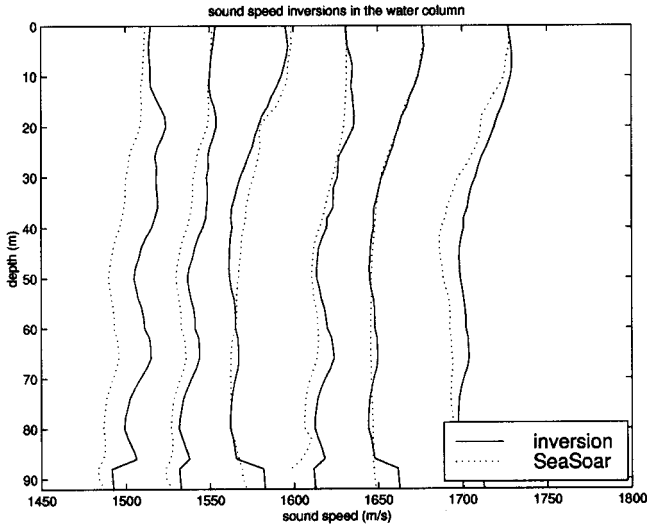

FIG. 14. Sound speeds in the water column obtained by GA inversion. The profiles at various sections are shown with sound-speed axis shifted by a small amount. Sound-speed profiles computed using SEASOAR data are also shown.

ity cores at locations 1, 2, and 3 (Fig. 7) and the range-independent inversion (Potty *et al.*, 2000) are also shown in that figure. Improvement in the inversion due to adiabatic modeling is evident, especially in the top 1 m of the sediment. Figure 14 shows the comparison of the sound speeds in the water column at six range points along the propagation path. Each profile is offset by 50 m/s for clarity of presentation, and hence only the difference between the two profiles is relevant. There is some disagreement between the two profiles, which is reflected in the group speed comparisons (Fig. 15). It should be noted that only four EOF coefficients were included to model the sound-speed fluctuations in the water column. Figure 15 shows the comparison of group speeds computed using the inversion and experimental data. Agreement is good for the late modal arrivals except for mode 1. There is appreciable difference in early arrivals, which may be due to the inferior ocean sound-speed values. It should also be noted that early arrivals are difficult to

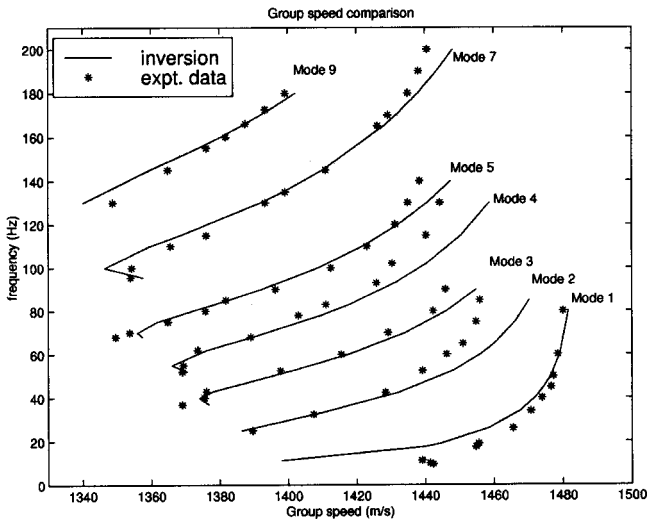

FIG. 15. Comparison of group speeds calculated using the inversion and experimental values of arrival times.

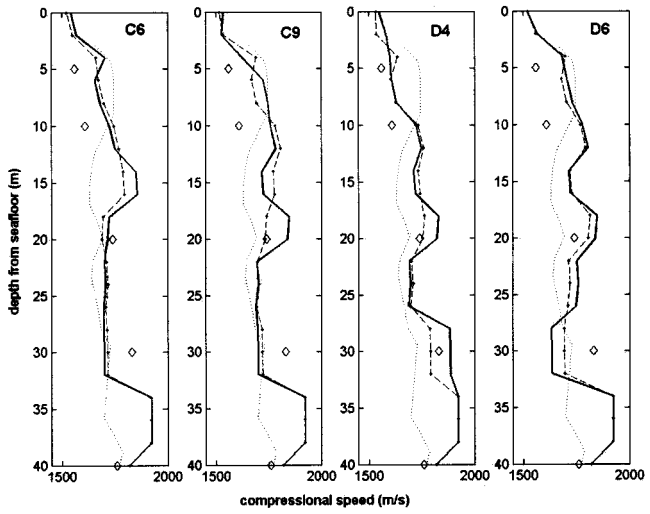

FIG. 16. Compressional speed profiles obtained by the inversion using SUS signals from D4, D6, C6, and C9. The continuous and dashed lines represent the sound-speed profile corresponding to the best and the mean inversions, respectively. The dotted line and the diamonds represent the AMCOR 6012 and 6010 data, respectively.

identify and separate and are prone to data errors compared to late arrivals. Later arrivals are more important to sediment inversions as they interact more with the bottom.

Figure 16 shows the compressional sound-speed profiles obtained by this inversion scheme using SUS signals corresponding to D4, D6, C6, and C9. The locations of these SUS charges are shown in Fig. 7. D4 and D6 belong to the downslope run, whereas the other two (C6 and C9) belong to the cross-slope run. The compressional wave speeds corresponding to the two AMCOR cores (6010 and 6012) are also shown in these figures. The variations in compressional wave speeds are not much, and in most cases they are within the standard errors. This was expected as the propagation paths for these four SUS signals are close to each other. Figure 17 shows the mean compressional speed profile on the shelf.

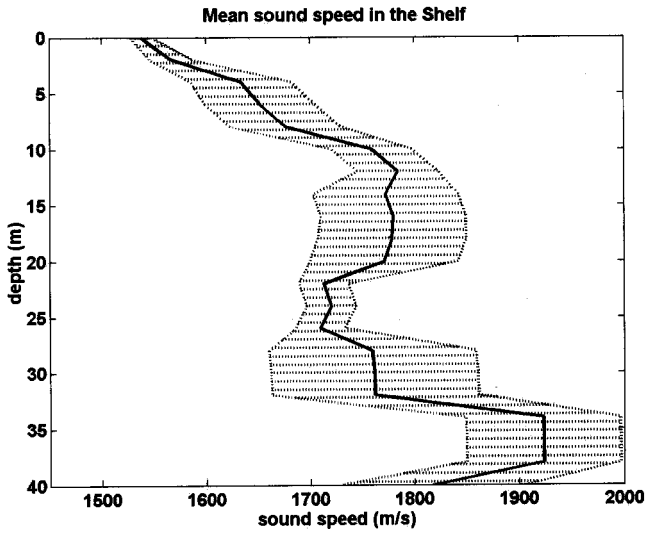

FIG. 17. Mean compressional speed profile in the shelf region. The shaded region corresponds to one standard deviation on either side of the mean. This mean profile is obtained using the inversions of SUS signals from various shots.

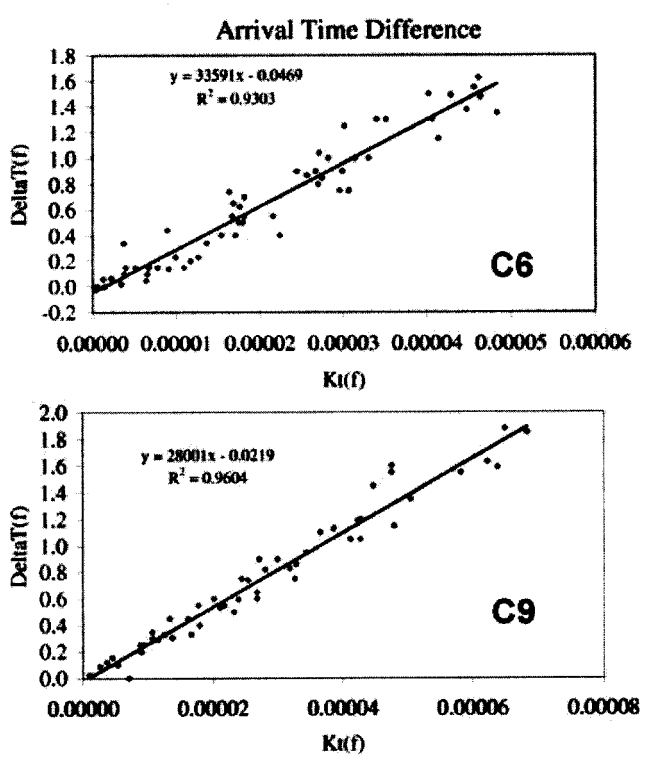

FIG. 18. Source–receiver range estimation for SUS charge C6 (top panel) and C9 (bottom panel). The estimated range is very close to the deployment range of 34.7 and 29.4 km, respectively. DeltaT(f)[$\Delta T(f)$] and $K_t(f)$ are defined in Sec. II C.

This mean profile is obtained using the inversion results corresponding to various SUS shots deployed in the shelf region. The mean compressional speed in the top 2 m of the sediment is of the order of 1550 m/s, which agrees well with the gravity core data. At greater depths the compressional speeds are of the order of 1700 m/s, which matches the average AMCOR-6012 data. The standard error in all the cases was of the order of 20–25 m/s in the top 15 to 20 m.

B. Source–receiver range estimation results

The differences in arrival times for various frequencies for a given mode and for various modes at a given frequency are calculated from the time–frequency distribution of the acoustic signal using Eqs. (5) and (6). The group speed values for various modes and frequencies are calculated using the compressional speed profile obtained from the adiabatic inversion. For two SUS charge explosions (C6 and C9), the experimental arrival time differences are plotted against the group slowness differences [Eqs. (5) and (6)]. It should be noted that these equations are strictly applicable only for range-independent propagation. The slopes of the lines obtained from these equations give the range for these SUS explosions (Fig. 18). The ranges were obtained as 33.6 and 28 km. These values are very close to the experimentally measured distance between the deployment locations of these SUS charges and the VLA (34.7 and 29.4 km, respectively). It should be noted that this estimation of range is based on range independence. The agreement between the estimated and actual ranges supports our assumption of range independence.

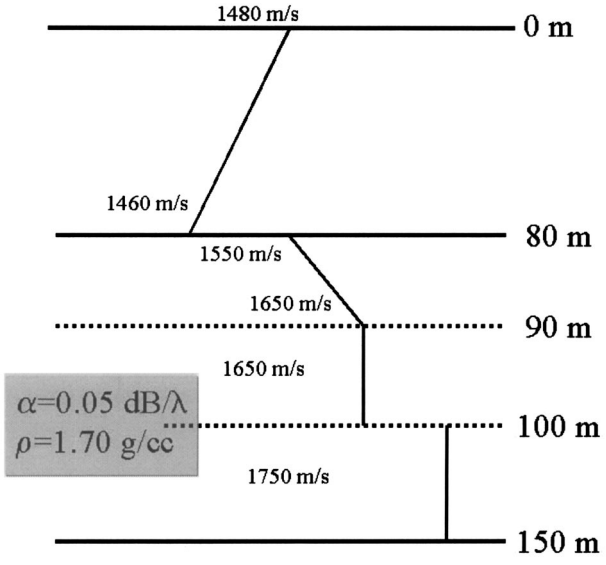

FIG. 19. Sound-speed profile used to generate synthetic time series for attenuation inversion.

C. Results of attenuation inversions: Inversion scheme II

1. Synthetic data

The inversion scheme II (Fig. 2) for obtaining the compressional wave attenuation was tested using synthetic data. Synthetic time series is generated for the sound-speed profile shown in Fig. 19. The attenuation coefficient for the sediment is assumed constant and equal to 0.05 dB/λ. Density also was assumed constant at 1.7 g/cc. The source was placed at a depth of 30 m and the receiver was at 40 km at a depth of 50 m. Acoustic pressure was generated for frequencies 10 to 200 Hz using the parabolic equation (PE)-based propagation code RAM (Collins, 1997). The time series thus obtained was analyzed using wavelets to separate individual mode arrivals. The arrivals obtained at 50 Hz are shown in Fig. 20. Modes 1, 2, and 3 can easily be identified in this figure. The ratios of pressure amplitudes are then calculated for use in the inversion scheme. Figure 21 shows the attenuation profile obtained using synthetic data. It can be noted that the inversion was successful in estimating the attenuation coefficient as the inversion closely matches the true attenuation value. It should also be noted that the synthetic data were noise-free and hence the spectral peaks were well separated and easily identifiable.

2. SUS data

This inversion scheme was next used to obtain the modal attenuation coefficients using the SUS data. The data from two explosions (D1 and D2) were chosen for this inversion. Signals received at the NE VLA at depths of 45.42, 53.12, 66.32, and 79.52 m were used. The propagation paths from these SUS explosions to the VLA are in a uniform depth of water and thus are assumed to be range indepen-

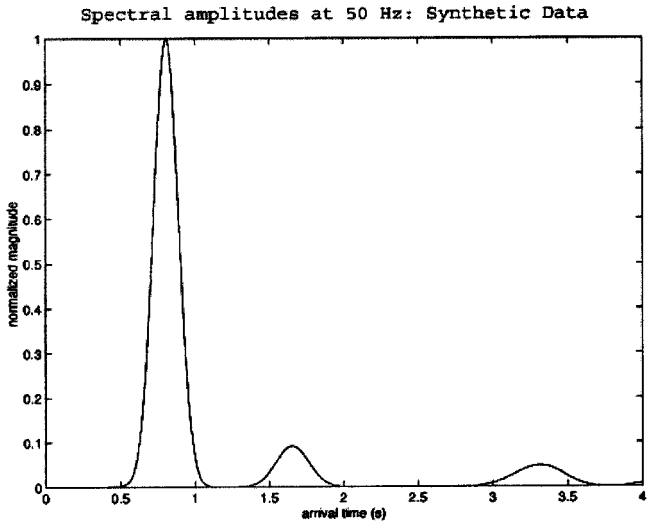

FIG. 20. Normalized magnitudes of the acoustic pressure for modes 1, 2, and 3 obtained using time–frequency analysis.

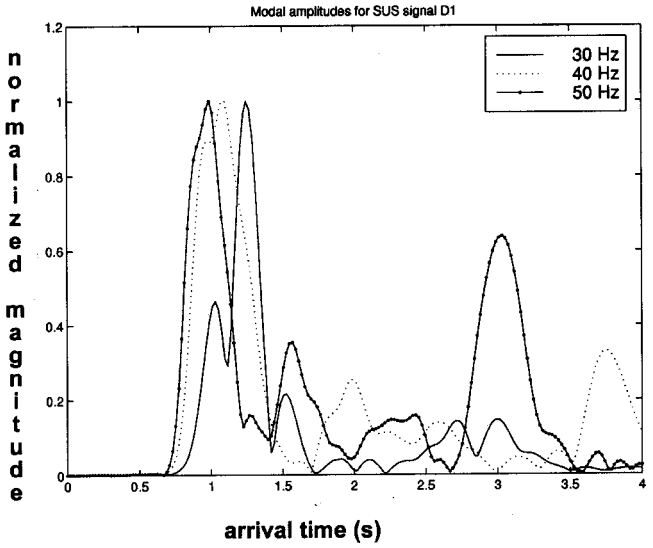

FIG. 22. Magnitudes of the acoustic pressure for SUS signal D1. Ratios between amplitudes of modes 1, 2, and 3 are used in the inversion scheme.

dent. This ignores any intrinsic medium range variability, which could be a source of some error. The time series from SUS D1 and D2 received at the VLA was analyzed using a Morlet wavelet. Figure 9 shows one such acoustic signal from SUS D2 received at the middle hydrophone at 66.32-m depth. Figure 10 shows the scalogram of this signal. It can be seen from this figure that in the 20- to 80-Hz region most of the acoustic energy is contained in the first three modes. Also, the first and second modes are well separated in this frequency band so that spectral ratios can be easily found. Figure 22 shows the normalized acoustic pressure amplitudes at frequencies 30, 40, and 50 Hz from the explosion D1. Spectral ratios R_{21}, R_{31}, and R_{32} are calculated using these mode amplitudes and are then used in the inversion to find the modal attenuation coefficients. It should be noted that at 70 Hz and higher, it is very difficult to identify the individual modal peaks, which makes the attenuation estimates less reliable at these frequencies. After obtaining the modal attenuation coefficients the attenuation profile $\alpha(z)$ was calculated by solving the integral equation (4). Inversion was carried out for frequencies in the range of 30–70 Hz and the results for frequency 30, 40, and 50 Hz are shown in Fig. 23. The attenuation profile calculated using gravity core data is also shown for comparison. Gravity core data are available only for a short depth of 1.5 to 2 m. The results agree reasonably well for the frequency shown in this figure and for other frequencies in the range 30–70 Hz. At higher frequencies the quality of the estimates becomes poor, which results in a comparatively larger disagreement. It should also be noted that the inversions corresponding to explosions D1 and D2 are in close agreement, as seen in the figure.

The attenuation coefficients are on the order of 0.04 to 0.045 dB/λ. In Fig. 24 the attenuation estimates (in dB/m) obtained by the present study are plotted along with previously available data reported by other investigators (Stoll, 1985). The shaded strip in this figure corresponds to the at-

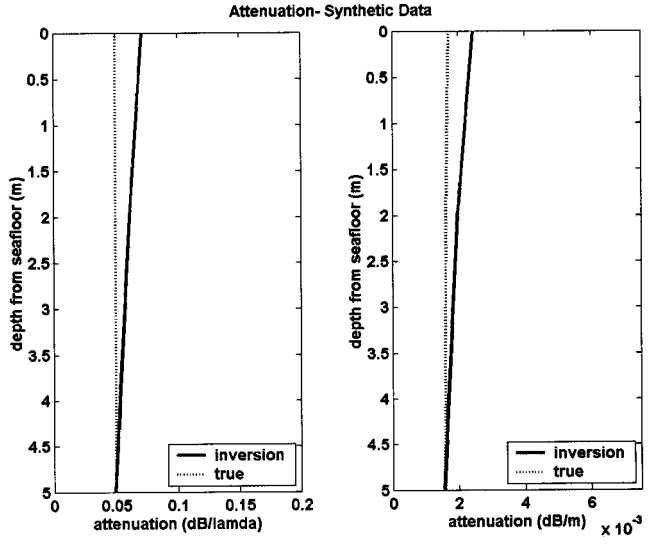

FIG. 21. Attenuation estimates obtained using the inversion scheme for the synthetic data. The true attenuation in this case was 0.05 dB/λ. Model attenuation coefficients were obtained from the inversion scheme and attenuation profile was estimated by linear inversion.

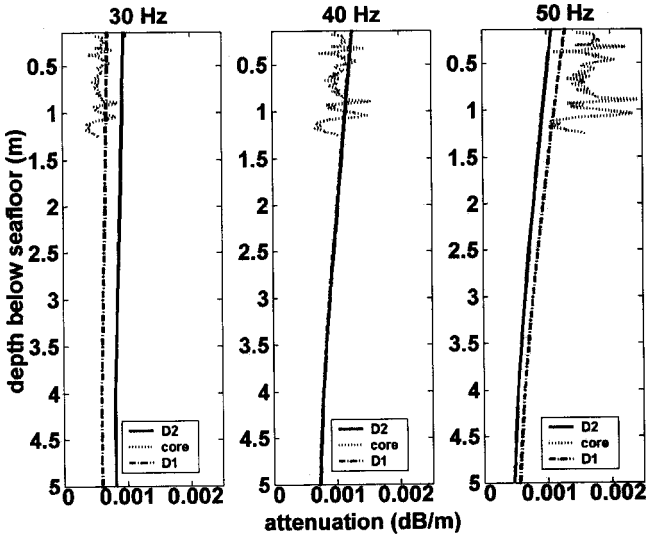

FIG. 23. Attenuation coefficient profile at 30, 40, and 50 Hz.

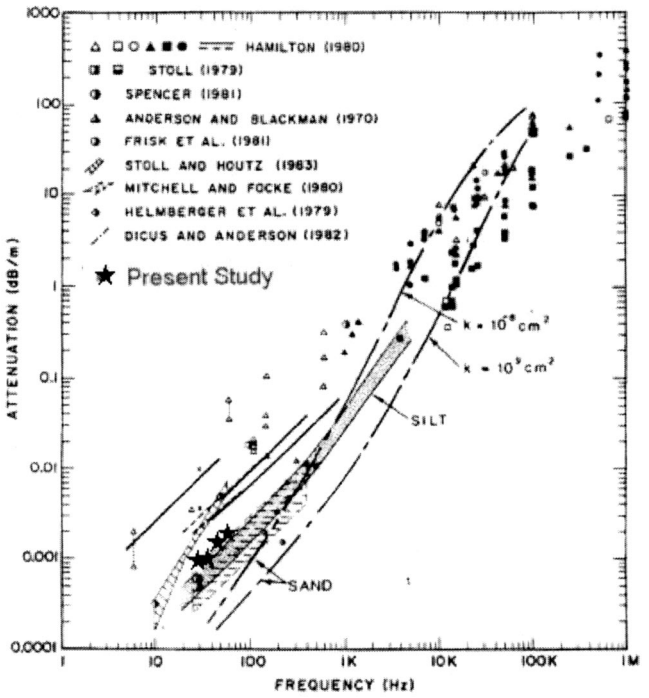

FIG. 24. Attenuation estimates (dB/m) obtained from present inversion. The historical data in the figure is taken from Stoll (1985).

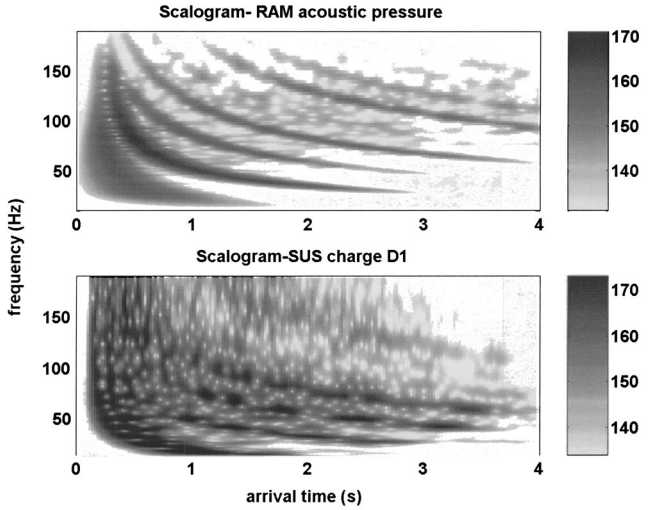

FIG. 25. Time–frequency diagrams of the synthetic and field data are shown in the top and bottom panels, respectively. The compressional wave speed and attenuation values from the inversion were used to generate the synthetic data.

tenuation values calculated using the Biot model (Badiey *et al.*, 1998) for sediments of the silt type. It should be noted that the amount of data at frequencies lower than 1 kHz is very small compared to higher frequencies. Values corresponding to our inversion range from 0.0009 to 0.0015 dB/m in the frequency range 30 to 70 Hz. These values are well below the values found by Hamilton (1972) for these frequencies. It should be noted that the Hamilton values were found by extrapolating the higher frequency findings based on linear first-power frequency dependence. If we calculate the value of attenuation coefficient with a value of $k=0.5$ (corresponding to very fine sand) from Hamilton (1972), and use the relationship

$$\alpha = k f^n \quad (n=1), \tag{21}$$

we get a value of 0.0025 dB/m for attenuation coefficient at a frequency of 50 Hz. The actual field values may be less than this since, in both sands and silts, the attenuation versus frequency relationship becomes nonlinear at low frequencies (Kibblewhite, 1989). This behavior is intimately related to the permeability of the sediment. Moreover, errors based on such extrapolation will be further compounded by the fact that, at low frequencies, propagation will also be controlled by deeper underlying structures rather than by the near-surface sediments alone. The vertical resolution length calculated was of the order of 4 m in the present inversion. The attenuation values then correspond to an average over a depth of 4 m, and surface sediments and deeper sandy sediments also. Another mechanism which can cause propagation at lower frequencies to be strongly attenuated is the presence of shear waves. However, this effect will be important only if the shear waves are on the order of 600 m/s. In the present study shear wave effects are probably not an important factor, as the shear speeds calculated using core data are on the order of 150 m/s.

Rogers *et al.* (1993), Mitchel and Focke (1983), and Zhao (1985) have reported attenuation values lower than Hamilton's predictions and closer to the present inversion. AMCOR-6010 site, which is southwest of the experimental location but in much shallower waters, consists of mostly silty sand silty clay overlying sand and a sandy clay layer. Rogers *et al.* (1993) have calculated the values of attenuation in the frequency range of 50 to 60 Hz from *in situ* measurements here. These values are 0.000 717 5 dB/m at 50 Hz and 0.001 09 dB/m at 75 Hz. Reflection data from the water–sediment interface measured by Mitchel and Focke (1983) yielded attenuation values of similar magnitude in deep ocean sediments in the 20–400-Hz frequency range. These values are also shown in Fig. 24. Zhao (1985) has reported a value of 0.0022 dB/m for attenuation coefficient at a site in the Yellow Sea off China's east coast at a water depth of 28.5 m. This value corresponds to a sand–silt–clay sediment at a frequency of 80 Hz. Even though these values correspond to different geographical locations, they all fall in the range of values closer to our inversion at these low frequencies.

Figure 25 shows the dispersion diagrams for synthetic data using the compressional speeds and attenuation obtained by the inversion. These are compared with the dispersion diagram for the experimental data. The synthetic data are noise-free and hence the individual modes are well separated. The first four modes are strong in both the real and synthetic data. Modes 5 and 6 are clearly identifiable in the synthetic data as these are noise-free as opposed to the real data. The pressure levels compare reasonably well. The source level for the explosive charge was evaluated using the method detailed by Urick (1983). The depths of receivers, depth of sources, and range obtained by the inversion are shown in Table I. They seem to agree well with the values noted at deployment.

TABLE I. Results of inversion scheme II using amplitude ratios.

Hydrophone number	Depth at deployment (m)	Depth-inversion (m)
1	45.42	44.60
4	53.12	52.00
8	66.32	65.30
12	79.52	79.59
Source depth (m)	18.29	18.62
Range (km)	40.96	40.82

VI. CONCLUSIONS

Sediment compressional speeds were evaluated using hybrid optimization schemes using broadband SUS data. Propagation was modeled using adiabatic mode theory. The inversions compare well with AMCOR and gravity core data. Compressional attenuation was obtained using another inversion scheme based on spectral ratios. This inversion scheme was tested using synthetically generated data. The attenuation values obtained fall within the reported compressional attenuation values in the frequency range 30–70 Hz. Source/receiver ranges were also estimated assuming approximate range independence, and agree well with measured values.

The possibilities of range variations in the bottom compressional wave speeds will be investigated further in another study. The up-slope propagation from the shots from the slope region will be more complicated because of the severe range variations in bathymetry, the range-dependent shelf break front, and probable variations in the bottom compressional wave speeds.

ACKNOWLEDGMENTS

The authors wish to thank the scientific team of the PRIMER experiment including Robert Beardsley, Ken Brink, Ching-Sang Chiu, Glen Gawarkiewicz, Robert Pickart, Alan Robinson, and Brian Sperry, Captain and Crew of R/V ENDEAVOR, and the pilots and crew from the Naval Air Warfare Center at Patuxent River NAS for their significant contributions to data collection and analysis. In particular, the authors recognize David Volak and Thomas Gabrielson for their contribution to the SUS component of the experimental design. This work was supported by Office of Naval Research, Dr. Jeffrey Simmen, Code 321 OA Program Manager and Dr. Steven Ramp, Code 322 PO Program Manager.

Badiey, M., Cheng, A. H.-D., and Mu, Y. (**1998**). ''From geology to geoacoustics—Evaluation of Biot–Stoll sound speed and attenuation for shallow water acoustics,'' J. Acoust. Soc. Am. **103**(1), 309–320.

Badiey, M., Jaya, I., and Cheng, A. (**1994**). ''Shallow water acoustic/geoacoustic experiments at the New Jersey Atlantic Generating Station site,'' J. Acoust. Soc. Am. **96**(6), 3593–3604.

Caiti, A., Akal, T., and Stoll, R. D. (**1994**). ''Estimation of shear wave velocity in shallow marine sediments,'' IEEE J. Ocean. Eng. **19**, 58–72.

Collins, M. D., Kuperman, W. A., and Schmidt, H. (**1992**). ''Nonlinear inversion for ocean-bottom properties,'' J. Acoust. Soc. Am. **92**, 2770–2783.

Collins, M. D. (**1997**). ''A split-step Pade solution for the parabolic equation method,'' J. Acoust. Soc. Am. **93**, 1736–1742.

Fletcher. (**1980**). *Practical Methods of Optimization* (Wiley, New York).

Gawarkiewicz, G., Bahr, F., Beardsley, R., and Brink, K. (**2001**). ''Interaction of a slope eddy with the shelfbreak front in the Middle Atlantic Bight,'' J. Phys. Oceanogr. **31**, 2783–2796.

Gerstoft, P. (**1994**). ''Inversion of seismoacoustic data using genetic algorithms and *a posteriori* probability distributions,'' J. Acoust. Soc. Am. **95**(2), 770–781.

Gerstoft, P., and Gingras, D. F. (**1996**). ''Parameter estimation using multifrequency range-dependent acoustic data in shallow water,'' J. Acoust. Soc. Am. **99**(5), 2839–2850.

Goldberg, D. (**1988**). *Genetic Algorithms* (Addison Wesley, Reading, MA).

Hamilton, E. L. (**1972**). ''Compressional wave attenuation in marine sediments,'' Geophysics **37**, 620–646.

Hamilton, E. L. (**1980**). ''Geoacoustic modeling of sea floor,'' J. Acoust. Soc. Am. **68**(5), 1313–1340.

Jensen, F. B., and Schmidt, H. (**1985**). ''Shear properties of ocean sediments determined from numerical modeling of Scholte wave data,'' in *Ocean Seismo-Acoustics*, edited by T. Akal and J. M. Berkson (Plenum, New York).

Kessel, R. T. (**1999**). ''A mode-based measure of field sensitivity to geoacoustic parameters in weakly range dependent environments,'' J. Acoust. Soc. Am. **105**(1), 122–129.

Kibblewhite, A. C. (**1989**). ''Attenuation of sound in marine sediments: A review with emphasis on new low frequency data,'' J. Acoust. Soc. Am. **86**, 716–738.

Lynch, J. F., Rajan, S. D., and Frisk, G. V. (**1991**). ''A comparison of broad band and narrow band modal inversions for bottom geoacoustic properties at a site near Corpus Christi, Texas,'' J. Acoust. Soc. Am. **89**(2), 648–665.

McGinnis, L. D., and Ottis, R. M. (**1979**). ''Compressional velocities from multichannel refraction arrivals on George's Bank-northwest Atlantic Ocean,'' Geophysics **44**, 1022–1032.

Mitchel, S., and Focke, K. (**1983**). ''The role of the sea bottom attenuation profile in the shallow water acoustic propagation,'' J. Acoust. Soc. Am. **73**, 465–473.

Porter, M. B., and Reiss, E. L. (**1984**). ''A numerical method for ocean acoustic normal modes,'' J. Acoust. Soc. Am. **76**(1), 244–252.

Potty, G., Miller, J. H., Lynch, J. F., and Smith, K. B. (**2000**). ''Tomographic mapping of sediments in shallow water,'' J. Acoust. Soc. Am. **108**(3), 973–986.

Rajan, S. D., Frisk, G. V., and Lynch, J. F. (**1992**). ''On the determination of modal attenuation coefficients and compressional wave attenuation profiles in a range dependent environment in Nantucket sound,'' IEEE J. Ocean. Eng. **17**(1), 118–127.

Rajan, S. D., Lynch, J. F., and Frisk, G. V. (**1987**). ''Perturbative inversion methods for obtaining bottom geoacoustic parameters in shallow water,'' J. Acoust. Soc. Am. **82**(3), 998–1017.

Rogers, A. K., Yamamoto, T., and Carey, W. (**1993**). ''Experimental investigation of sediment effect on acoustic wave propagation in the shallow ocean,'' J. Acoust. Soc. Am. **93**, 1747–1761.

Sen, M., and Stoffa, P. L. (**1995**). *Global Optimization Methods in Geophysical Inversion* (Elsevier, Amsterdam).

Siderius, M., Gerstoft, P., and Nielsen, P. (**1998**). ''Broadband geo-acoustic inversion from sparse data by Genetic Algorithms,'' J. Comput. Acoust. **6**, 117–134.

Stoll, R. D. (**1985**). ''Marine sediment acoustics,'' J. Acoust. Soc. Am. **77**(5), 1789–1799.

Stoll, R. D., Bryan, G. M., and Bautista, E. O. (**1994**). ''Measuring lateral variability of sediment geoacoustic properties,'' J. Acoust. Soc. Am. **96**(1), 427–438.

Taroudakis, M. I., and Markaki, M. G. (**1997**). ''On the use of matched-field processing and hybrid algorithms for vertical slice tomography,'' J. Acoust. Soc. Am. **102**(2), 885–895.

Tindle, C. T. (**1982**). ''Attenuation parameters from normal mode measurements,'' J. Acoust. Soc. Am. **71**(5), 1145–1148.

Tolstoy, A., Diachok, O., and Frazer, L. N. (**1991**). ''Acoustic tomography via matched field processing,'' J. Acoust. Soc. Am. **89**(3), 1119–1127.

Trevorrow, M. V., and Yamamoto, T. (**1991**). ''Summary of marine sedimentary shear modulus and acoustic speed profile results using gravity wave inversion technique,'' J. Acoust. Soc. Am. **90**(1), 441–456.

Urick, R. J. (**1983**). *Principles of Underwater Sound for Engineers* (McGraw-Hill, New York).

Zhao, J. (**1985**). ''Normal mode measurements and remote sensing of sea bottom sound velocity and attenuation in shallow water,'' J. Acoust. Soc. Am. **78**(3), 1003–1009.

Zhou, J., Zhang, X., Rogers, P. H., and Jarzynski, J. (**1987**). ''Geoacoustic parameters in a stratified sea bottom from shallow water acoustic propagation,'' J. Acoust. Soc. Am. **82**(6), 2068–2074.